Estimating Regional Myocardial Contraction Using Miniature Transducers on the Epicardium

Thuy Thu Nguyen[1], Andreas W. Espinoza[2,3], Stefan Hyler[3], Espen W. Remme[4], Jan D'hooge[5] & Lars Hoff[1]

[1] Institutt for mikrosystemer - Universitetet i Sørøst-Norge
[2] Avdeling for anestesiologi - Oslo universitetssykehus HF
[3]Intervensjonssenteret - Oslo universitetssykehus HF
[4] Institutt kir. forskning, Rikshospitalet - Oslo universitetssykehus HF
[5]KU Leuven - University of Leuven

Accepted version of an article in:
Ultrasound in Medicine and Biology

Publisher's version: Nguyen, T. T., Espinoza, A. W., Hyler, S., Remme, E. W., D'hooge, J. & Hoff, L. (2019). Estimating Regional Myocardial Contraction Using Miniature Transducers on the Epicardium. *Ultrasound in Medicine & Biology, 45*(11), 2958-2969.
https://doi.org/10.1016/j.ultrasmedbio.2019.07.416

Estimating Regional Myocardial Contraction Using Miniature Transducers on the Epicardium

Thuy Thu Nguyen[a], Andreas W. Espinoza[b,c], Stefan Hyler[b], Espen W. Remme[d], Jan D'hooge[e], Lars Hoff[a]

[a]Dept. of Microsystems, University of South-Eastern Norway, Horten, Norway.

[b]The Intervention Centre and [c]Dept.of Anaesthesiology, Oslo University Hospital, Rikshospitalet, Oslo, Norway.

[d]Institute for Surgical Research, Oslo University Hospital, Rikshospitalet, Oslo, Norway.

[e]Lab. on Cardiovascular Imaging & Dynamics, Dept. of Cardiovascular Diseases, Catholic University of Leuven, Leuven, Belgium.

Thuy Thu Nguyen

University of South-Eastern Norway, Postboks 4, 3199 Borre, Norway

Phone: +47 403 37910

Email: tng@usn.no

Abstract

This paper describes an ultrasound system to monitor cardiac motion using miniature transducers attached directly to the epicardial surface. The aim is both as a research tool for detailed studies of cardiac mechanics, and to develop a continuous, real time system for perioperative evaluation of heart function. The system was tested on a porcine model. Two 3 mm diameter, 10 MHz ultrasound transducers were sutured to the epicardial surface. As the epicardial surface is the reference for the velocity and strain estimations, this procedure compensates for the motion of the heart. The short distance allows use of high frequencies and pulse repetition rates. The system was driven in pulse-echo mode, using electronics developed for the application, and RF-lines were recorded at pulse repetition rate 2500 s^{-1}. The endocardial border was detected using an algorithm based on fuzzy logic with filtering to reduce noise and remove outliers, and the myocardium was divided into 4 layers. Inside the myocardium, radial tissue velocity as function of depth was calculated from the recorded RF signals, and the velocity estimates were used to estimate radial strain rate and strain, and to track the motion of the myocardial layers. The scope of this paper is technical, giving a detailed description of system design, hardware electronics, and algorithms, with examples of processed velocity patterns and myocardial strain curves. The results from a study on a porcine model demonstrate the system's ability to estimate myocardial velocity and strain patterns and to track the motion of the myocardial layers, thereby obtaining detailed information of the regional function of the myocardium.

Keywords: Ultrasound, strain, tissue velocity, myocardium, pig, miniature transducer, perioperative monitoring.

Introduction

Reliable methods to assess ventricular function during and after cardiac surgery are essential tools to evaluate patient prognosis (Landesberg et al. 2001; Espinoza et al. 2011). The most common method for monitoring heart status is the electrocardiogram (ECG). ECG is an invaluable tool for heart monitoring, but the sensitivity for detecting an occlusion or ischemia is regarded as low (Comunale et al. 1998; Crescenzi et al. 2004; Smith et al. 1985). ECG and hemodynamic monitoring address the global heart function, and are used as low-threshold, continuous first-line monitoring methods (Ludbrook et al. 1993). Tissue Doppler echocardiography is a more specific and quantitative tool for the assessment of cardiac function, being able to measure regional tissue velocity and displacement in the myocardium (Skulstad et al. 2006; Yu et al. 2007). But cardiac ultrasound systems are primarily designed for intermittent imaging, not for continuous monitoring. Small single-element ultrasound transducers attached directly to the heart surface provide an alternative option for continuous heart monitoring. Ellis et al. (Ellis et al. 1956) used *sonocardiometry* to measure left ventricular (LV) diameter continuously. In this technique, two transducers were attached to the heart surface, one as transmitter, the other as receiver, and the method was used to measure local dimensional changes of the myocardium (Bugge-Asperheim et al. 1969). This is a valuable research tool, but too invasive for monitoring patients during cardiac surgery, and it does not provide local information of strain inside the myocardium. Hartley et al. demonstrated a method using one single-element transducer on the epicardium in a pulse-echo technique, to measure myocardial thickening (Hartley et al. 1983). We developed this method further, attaching miniature ultrasound transducers to the epicardium, measuring myocardial velocities (Hoff et al. 2008; Nguyen et al. 2011).

The myocardial deformation, represented by myocardial strain, reflects the work load of the myocardium, and the strain is therefore a suitable quantitative parameter characterizing the myocardial function (D'hooge et al. 2000; Kowalski et al. 2001; Kukulski et al. 2002; Kukulski et al. 2003; Weidemann et al. 2002). Cardiac mechanics is complicated and still not completely understood. For example, most studies of the distribution of radial strain across the LV wall show increasing strain values from the epicardial layer to the endocardial layer (Matre et al. 2005), while others show the

highest strain in the mid-myocardium (D'hooge et al. 2001). Computer models using the Finite Element Model to simulate the LV contraction indicate that transmural layer strain depends on the local curvature of the investigated segment (Choi et al. 2010; Choi et al. 2011). Studies have also showed that there is a link between ischemia and changes in radial strain (Matre et al. 2007; Skulstad et al. 2006). Hence, detailed measurements of ventricular motion are of great interest to better understand the details in the heart mechanics, and may contribute to improve heart disease diagnosis.

This paper builds on the previously described methods using miniature transducers attached to the heart surface, developing these further to monitor cardiac motion, most notably strain, as function of depth into the myocardium. Two transducers were attached to the epicardium and used in pulse-echo mode, and results were processed to find velocity, strain, and displacement as function of depth into the myocardium. Compared to transthoracic ultrasound, our approach uses transducers that move with the heart surface, using the epicardium as reference for the velocity calculations, thereby compensating for the heart's own movements. This can be beneficial for strain and strain rate measurements, which are based on small velocity differences within the myocardium. In conventional echocardiography, parts of the myocardial tissue move in and out of the imaging plane, causing problems in the interpretation. Furthermore, the short depth allows higher frequency and higher pulse repetition frequency, allowing improvement in spatial and temporal resolution (Nguyen et al. 2011). The proposed clinical application of this system is two-fold: The long-time goal is to develop a small, dedicated system to continuously monitor regional cardiac function during and after cardiac surgery. This should have faster response time and better sensitivity and specificity than ECG, and operate continuously, perhaps for several days, with minimal operator interaction. It should also be smaller, simpler and less expensive than conventional cardiac ultrasound scanners. Secondly, as a shorter-term goal, this system's high spatial and temporal resolution, inherit compensation for the heart's own movements, and continuous capabilities make it suited as a research tool for fundamental studies of heart mechanics. It can give continuous detailed measurements of the heart's contraction pattern and regional strain distribution over longer periods, on a level not easily achieved by conventional ultrasound systems.

Sensors that can track myocardial motion, may be used to detect motion abnormalities and give early warning of potential complications occurring during surgery such as ischemia. Motion changes appear before changes detected by other methods such as ECG. This has been demonstrated in patients and in animal experiments (Espinoza et al. 2011; Hyler et al. 2015). We, and others, have found an immediate reduction in systolic wall thickening velocities, together with an increase in early diastolic wall thickening (post-systolic wall thickening). Ischemia can result from obstruction in blood flow in the bypass grafts from various reasons, such as thrombosis, kinking of graft or even wide retraction of the sternum retractor (Espinoza et al. 2012). The early warning of such blood flow impediments can give the surgeon time to correct the underlying cause before chest closure.

The data acquisition system is identical to the one used by Espinoza et al. (Espinoza et al. 2011). The present paper gives more detail on the technology, which was not so thoroughly described in this purely clinical paper. Further, Espinoza et al. (Espinoza et al. 2011) used a pulse Doppler estimator to find the velocity at a fixed depth. This has been extended to calculate velocity at all depths, and combine these data with boundary detection and tissue tracking algorithms, allowing us to track myocardial layer motion and estimate strain in the myocardial layers, with example measurements on an open thorax porcine model.

Materials and Methods

Animal Experiment Procedure

The ultrasound system was tested in open chest porcine experiment. The ultrasound recording was obtained in a study previously published (Hyler et al. 2015). The use of animals in that study was approved by National Animal Research Authority in Norway (No. 27/09-1747). The handling of the animals was in accordance with institutional guidelines, and national and international regulations. The re-use of the recordings in this study is in accordance with the Three R's, to reduce the number of animals used in research (Directive 2010/63/EU). Two sensors were sutured to the epicardial surface of the left ventricle in the apical region, near the intervention area, and in the basal region, far from the intervention area, as shown in Figure 1. The sensors had to be placed at stable positions. ECG and LV

blood pressure were recorded concurrently and synchronized with the ultrasound measurement from the surface of the left ventricle.

Transducers, Electronics and Data Acquisition

A brief description of an earlier version of this system can be found in (Hoff et al. 2008). A schematic drawing is shown in Figure 2. The system consisted of a two-channel ultrasound transmit-receive system built in-house from state of the art electronic components. This was connected to two single element transducers sutured to the epicardium of the LV wall. The results were sampled by a high-speed data acquisition board, and stored on a computer disk. The system employed custom-build single-element transducers (Imasonic SAS, Besancon, France). The transducers have 3 mm active diameter, center frequency 10 MHz, 60% bandwidth, and are focused geometrically to 20 mm. In each experiment, two such transducers were sutured to the epicardium of the LV wall, at two different positions. Ferrite ring transformers at ratio 9:4 were connected between the transducers and the rest of the equipment to provide galvanic isolation for electric safety, with the additional benefit of improving the electrical impedance matching from the transmit electronics to the transducer. The two transducers were excited simultaneously, and the received echoes were split into two separate receive channels in the transmit/receive switch. The transducers were mounted so that the distance between them was larger than twice the maximum imaging depth, ensuring that the receiving was finished before the direct wave from one transducer reached the other to avoid interference between the two transducers.

The analog electronics for the ultrasound transmit-receive system was assembled in-house using evaluation boards from electronics manufacturers. The transmitter was based on a Supertex MD1210DB1 evaluation board (Microchip Technology, Chandler, AZ, USA), programmed to transmit short pulses of center frequency 10 MHz at repetition rate 2500 pulses/s. The transmit voltage was set to ±18V. The MD1210DB1 evaluation board was modified by decreasing the output protection resistor to 22 Ω, increasing the transmitted power while still giving sufficient short-circuit protection, and the internal oscillator was disabled. Clock signals were taken from an external oscillator, to obtain phase synchronization between the transmitted ultrasound pulses and the sampling of the echoes.

A two-channel passive transmit-receive switch was implemented by using a diode network. The transmit pulses were simultaneously sent to the two transducers, whereas the received echoes from the two transducers were separated and directed to the receiving amplifier.

Timing and sampling were controlled by an external oscillator (IQXO-350C, IQD Ltd., Somerset, England), running at four times the transmit frequency, i.e. 40 MHz. The transducers were driven by two-cycle symmetric square wave pulses, generated by dividing the oscillator clock frequency by four, and the pulse repetition frequency was fixed to 1/4000 of the center frequency, giving a pulse repetition rate of 2500 pulses/s. Echoes received from the myocardium were amplified in a dual-channel ultra-low noise amplifier, AD8332-EVALZ (Analog Devices Inc., Norwood, MA, USA) and sampled by a high-speed 14 bit digitizer board (NI-PCI 5122, National Instruments Inc., Austin, TX, USA), placed on the PCI-bus of a desktop personal computer. The external 40 MHz oscillator was also used to control the sampling, to avoid jitter between the transmitted and received signals, giving sample rate 40 MS/s. The system was controlled by software written in-house using LabWIEW (National Instruments Inc.), controlling the acquisition and processing of the echoes. During operation, the results were displayed in real-time on the computer screen, both as wall thickness (M-mode) images over time, and as tissue velocity at a fixed depth. Unprocessed RF-lines were streamed to disk during selected time intervals for detailed processing and evaluation off-line. These stored scanlines were used in the calculations presented in this paper. A user-friendly graphical user interface was designed to control the operation of the system.

To support the ultrasound data, ECG and blood pressure were registered synchronously with the ultrasound measurements using separate analog input channels in the low-speed multi-function DAQ, operating at rate 500 Samples/s. In the experiment described in this paper, the main purpose of these signals was to provide time references for the cardiac cycle. ECG signals were registered by a Siemens SC 9000XL monitor (Siemens, AG, Erlangen, Germany) and the analog output from this monitor was sampled by a separate 16-bit digitizer board (NI-USB 6211, National Instruments Inc.). The delay in the analog ECG unit was measured using a signal generator and an oscilloscope to 21.5 ms, and this was compensated in the processing and display. Instantaneous blood pressures at up to three different

positions were measured invasively by three Millar MPC-500 Mikro-Tip Pressure Transducer Catheters, connected to Millar TC-510 Pressure Control Units (Millar Instrument, Houston, TX, USA). The locations of the three pressure catheters varied between different experiments, but in most cases, they were positioned in the aorta, left ventricle and left atrium. The microvolt signals from the TC-510 control units were amplified 400 times and bandwidth-limited to 100 Hz by in-house developed electronics designed around INA101 instrumentation amplifiers (Texas Instruments Inc, Dallas, TX, USA). The outputs from these amplifiers were sampled simultaneously with the ECG signals, using the same AD-board. The amplifier circuits used to amplify the pressure catheter signals showed no delay. Synchronization between the low-speed digitizer for ECG and pressure and the high-speed digitizer for ultrasound signals was achieved by letting an analog output in the low-speed DAQ control the analog gain in the ultrasound pre-amplifier. This gain control responds fast enough to control the TGC. This gain was set briefly to zero at start of the recordings, creating a brief lack of signal in the received ultrasound signals. By this procedure, synchronization between the pressure and ECG-signals and the ultrasound recordings was achieved at precision limited by the sample interval of the low-speed digitizer, i.e. 2 ms.

Data processing

The received echoes were saved to disk as raw, unprocessed RF-scanlines. These scanlines were loaded into Matlab (The MathWorks Inc., Natick, MA, USA) for estimating the myocardial velocity, strain and strain rate relative to the transducer, as function of distance.

M-mode images were rebuilt from the recorded RF signals, using the Hilbert transform for envelope detection. The M-mode images served mainly as background maps to define the position of the endocardium and the myocardial depths for estimating strain. The endocardial border was found by a boundary detection algorithm, based on fuzzy logic, and moved 1.5 mm inwards to avoid boundary effects. A thin layer beneath the epicardial surface was omitted to avoid near-field artifacts. The thickness of this layer was 4 mm in the apical region and 3.5 mm in the basal region. End-diastole was determined as the onset of the R-wave in the ECG recordings. Segmentation into myocardial layers was done at end-diastole, where the myocardial wall was divided into n equally sized layers, from the

epicardium to the detected endocardial border. The number of myocardial layers n, giving the layer thickness, could be chosen as a balance between spatial resolution and noise, and was in this study selected to n=4.

The motion of each layer was determined by tracking the velocity forward and backward over one cardiac cycle. A weighted average of the forward and backward tracking results was used to compensate for drift. Radial strain rate was computed as the spatial velocity gradient, estimated from linear regression within each layer, and the radial strain for each layer was found by temporal integration of the strain rate. The end-diastolic strain was set to zero at each heart cycle, as the heart should return to initial state before a new cycle (D'hooge et al. 2000). It should be pointed out that reliable velocity estimates and endocardial boundary detection are essential to obtain good radial strain estimates.

Velocity Estimations

Figure 3 illustrates the flow chart of velocity estimation. Local velocity was estimated from the acquired RF-lines. These were first filtered using a zero-phase 4th order bandpass Butterworth filter centered around the transmit frequency, to remove noise. Tissue velocities were then estimated from the RF signals by using cross-correlation to estimate the time-delay between successive scanlines. Cross-correlation is an established tracking method to obtain a high signal to noise ratio, however, this method reduces the spatial resolution, and is computationally very heavy. The accuracy of the time delay estimates, and consequently, the velocity estimates, was improved by first up-sampling the RF signals a factor R=10 using a FIR-filter based interpolation method, before the cross-correlation was calculated (Nguyen et al. 2011). Then, the estimate for the position of the peak in the cross-correlation curves was improved by using sub-sample interpolation applying a parabolic-fit (Céspedes et al. 1995). Cross-correlation between successive scanlines was done using a kernel size corresponding to 616 µm, or 4λ, with 50% overlap. Here, $\lambda=c/f$ is the wavelength of the transmitted pulses, c is the speed of sound, and f is the center frequency of the transmitted pulses. The displacement between two consecutive RF-lines was restricted within the interval [-λ/2 λ/2], giving a maximum detectable velocity $v_{max} = \frac{c\, f_{PR}}{2f}$

=192.5 mm/s. The minimum detectable velocity was $v_{min} = \frac{c\, f_{PR}}{R f_s}$ = 9.625 mm/s where f_{PR} is the pulse repetition frequency, and f_s is the sample rate.

Endocardial boundary detection

The deepest layer in these estimations is limited by the endocardial border. Inside the myocardium, the layers are tracked based on the velocity estimates, but the endocardial border is better tracked based on the large differences in echo strength between blood and myocardial tissue. Several boundary detection methods for two-dimensional echocardiographic images have been presented in the literature (Alshennawy and Aly 2009; Chu et al. 1988; Feng et al. 1991; Setarehdan and Soraghan 1999), mainly based on the intensity of the M-mode image. The method used in this paper was described by Abdallah et al. (Alshennawy and Aly 2009), using a fuzzy logic technique to determine the image edges. A block diagram of the method used to detect endocardial border is shown in Figure 4. The estimate for the endocardial boundary determined from these image edges was then improved by filtering in the time direction and employing a snake algorithm (Kass et al. 1988) in the time direction to smoothen the curve.

On our data, the robustness of the endocardial border detection obtained from this fuzzy logic technique was found to be better than a conventional edge detection method using the Sobel operator, in line with the results from (Alshennawy and Aly 2009). Instead of having only true or false values as Boolean logic, the membership value in Fuzzy logic varies continuously between 0 and 1. The membership function is a curve used to calculate the membership values for pixels from the gray scale M-mode image as shown in Figure 5. The fuzzy system rules given in (Alshennawy and Aly 2009) based on the membership values of pixels in a 3x3 mask were used to detect the boundary. The range of the M-mode image was mapped to gray scale of range [0 255] as shown in Figure 6. The results were found to be sensitive to the thresholds *a* and *b* used to determine whether a pixel is black or white, and these parameters had to be adjusted for each M-mode image. In the following example, the thresholds were set to *a*=140.25 and *b*=214.2. After fuzzy logic step, the gray scale M-mode image became an image which has “white” pixels at the boundary and “black” pixels at the other positions.

This fuzzy logic method will detect the boundaries of the myocardial fibers. In this study, it was only applied to find the endocardial border. A depth range limiting the search for the endocardial boundary was defined from 10 mm to 19.98 mm. The processed M-mode lines were scanned using the fuzzy logic algorithm, and the boundary determined as the last 'white' points in the depth. The blue line in Figure 7a shows the endocardial boundary detected by the Fuzzy logic processing and boundary search steps, before further processing. A maximum filter of length 7 was then applied to the detected endocardial border, as a function of time, to remove noise, resulting in the red line in Figure 7a. The maximum filter is defined as a transformation which replaces the value of the first element with the maximum value of all the elements within the running window:

$$z_b(i) = \max(z_b(i), z_b(i+1), \dots, z_b(i+n-1)) \quad (1)$$

where $z_b(i)$ is the position of the border at discrete time *i* and *n* is the length of the filter. *n* is an integer. The result in Fig.7a demonstrates how this maximum filter effectively removed spikes in the original estimate.

After the maximum filter, the boundary estimate still contained points suspected to be outliers. These were removed by requiring the distance in the depth direction between two successive points in the boundary to be smaller or equal to the maximum velocity at that time, multiplied by the pulse repetition interval. Maximum velocity at a time is defined as the maximum velocity along the depth at that time, given by the velocity estimator described previously. As a final step, the myocardium expands monotonically during systole, and this requirement was applied to improve the results further, removing the last outliers. After applying these steps, the snake algorithm (Kass et al. 1988) was employed to smoothen the boundary along the time. The snake parameters were set to α=5000, β=0, step size γ=10, and was run over 500 iterations. The result after applying the snake algorithm is shown in Figure 7b, as the red line. This can be compared with the result before applying the algorithm, the blue line in Figure 7a. Figure 7b also compares the result with (red line) and without (blue line) requiring monotonous expansion during systole. In this example, we believe the endocardial border determined with assuming monotonous expansion during systole is slightly more accurate than without assuming monotonous

expansion, see around 4.68 second in Figure 7b. However, the ground truth is not known, and this must be viewed as an assumption based on the shape of the curves and the M-mode image.

Results

The received scanlines were processed to M-mode images, and these were used to divide the myocardium into four layers at end-diastole. The results are shown in Figures 8 to 11. In these figures, the end-systole is marked with blue vertical lines, and the end-diastole with magenta lines. Synchronously recorded ECG and LV pressure curves were used for timing, primarily to identify end-diastole and end-systole. Note that the RF data analyzed in Figures 8 to 11 were acquired during a study where the animal had been exposed to previous interventions, and the curves may not be representative of a healthy, undisturbed myocardium. Table 1 shows the parameters used in the fuzzy logic endocardial boundary detection algorithm, based on the intensity of M-mode images. The resulting estimated radial velocity patterns in the myocardium are displayed as color-plots in Figure 8, for the two transducers. The results in Figure 8 were calculated without any filtering of the velocity. These velocities were used to calculate the motion of the four myocardial layers. Figure 9 shows the calculated motion of the myocardial layers by tracking the motion in the forward direction only, while Figure 10 shows the motion of the layers by using both forward and backward tracking in order to compensate for drift seen in Figure 9. The detected endocardial border is displayed together with the myocardial layers in Figures 9 and 10.

The motion of the myocardium is close to periodic, and can be assumed to return to its initial state after each cardiac cycle. From the results, we notice that little noise is seen in Figure 8. Likewise, very little apparent drift is seen in the tracked layers in Figure 9, as the layers seem to return to their initial position after each cardiac cycle. The M-mode images and forward estimated velocity images show that the data near the apex contain somewhat more noise than the data near the base. Close examination of the tracked layers indicates that there is some drift in the layers tracked near the apex, but considerably less in the curves tracked near the base. The drifts are 0.19 mm for lower boundary and 0.1 mm for the upper boundary for the 4^{th} layer of myocardium in apical region at end-diastole, at 4.485 second, in Figure 9 by using only forward tracking as the thickness of the layer is 1.73 mm at end-diastole.

The radial strain rate was calculated as the gradient of the estimated velocities along the depth. This radial strain rate was integrated temporally to obtain the radial strain, the result is shown in Figure 11. One curve is shown for each of the four myocardial layers, numbered from layer 1 at sub-epicardium to layer 4 at sub-endocardium. From Figure 11, it is seen that the radial strain repeats itself periodically every heart cycle, as should be expected. In the recordings from the base of the heart, the strain curves from the different myocardial layers have almost identical shapes. In contrast to this, the recordings from the apex show substantial variation between the strain curves calculated from different myocardial layers. The reason for these differences is not clear, but it should be noted that the animal model had been exposed to various interventions and handling prior to this recording, mainly affecting the apical region. This might explain the differences in shape between results from the base and apex, but further studies involving several animals and interventions are needed to draw any conclusion about this.

Discussion

The aim of this study was to demonstrate a miniaturized, simple system to continuously monitor strain inside the myocardium. The method offers several advantages for high signal quality compared to conventional non-invasive ultrasound imaging. First, the method by design compensates for the heart's own motion, and is ideally only sensitive to the myocardial contraction. In addition, the sound pulses do not have to penetrate the thorax wall, giving a short distance to the region of interest, and low attenuation. This allows higher pulse repetition rate and higher frequency, offering better temporal and spatial resolution than conventional ultrasound imaging. This study used a pulse repetition rate of 2500 pulses/s and frequency 10 MHz, but these are conservative choices that may be increased.

The 10 MHz transducers attached directly to the myocardium gave low noise raw data of sufficient resolution in space and time to allow reliable tracking the motion of the myocardial layers. The velocity estimates found from these raw RF scanlines are the basis for the following calculations. Hence, robust velocity estimators are essential for all further computations such as layer tracking, strain rate and strain estimates. We found the cross-correlation between successive RF-lines to yield robust and reproducible velocity data, although a reference to a gold standard for myocardial velocity is not available in this setting. An indication of the robustness of the method is that the forward tracking in Figure 9 ended

very close to the first tracking point of the next cycle, even though no filter was applied to the velocity estimates. This was true for both data sets, i.e. from the apex and from the base. A check on reproducibility and drift in the system was done by tracking the myocardial layer motion both forwards and backwards, and comparing the results. This is shown in Figure 9, where differences were found negligible, demonstrating very little drift in the tracking algorithm.

The maximum absolute myocardial velocity detected during this study was 100 mm/s, see Figure 8. This is smaller than maximum velocity of the phase shift estimator, 192.5 mm/s, defined by limiting the displacement of consecutive RF lines to be within the interval $[-\lambda/2\ \lambda/2]$. Hence, aliasing was not a problem with the settings used in this study. In a previous study (Nguyen et al. 2011), we used the Snake regularization (Kass et al. 1988) to reduce noise and remove outliers from the curves. This is a computationally heavy method. In the present study, outliers were not a problem, and no filter was applied to the estimated velocities. However, a low pass Butterworth filter could be used to reduce noise. This required less computations than the Snake regularization, allowing faster calculations.

The endocardial boundary detection was based on Fuzzy logic supported by a combination of a maximum filter, removal of outliers, and snake regularization. The result, in Figure 7, indicates that this procedure was able to track the endocardial border well. Some further improvement could be achieved by in addition requiring monotonous expansion during systole see Figure 7b, but this difference is not dramatic. The apparent improvement achieved by this requirement must be weighed against the risk of imposing too strict restrictions to the myocardial motion. This border detection method does not work well when the border is too close to the edge of the image, as the method organizes pixels in a 3x3 mask. This can explain why the detected border seems to deviate from the actual endocardial border around end-systole in Figure 7.

Strain measurements are susceptible to noise, and careful signal processing is crucial to obtain reliable strain estimates. The radial strain in Figure 11 shows different behaviour of myocardium at two different regions.

The long-term goal of this study is to develop a monitoring tool for patients during and after cardiac surgery. However, it can also be useful as a research tool for fundamental studies, offering detailed

information on heart mechanics. The prototype sensors used in these experiments are too large to be removed after chest closure. In future versions, the transducers may be thinned down to the shape of a thin disc, preserving the 2 to 3 mm diameter acoustic aperture, but reducing the thickness. This could allow the sensors to be removed after chest closure similar to removal of temporary pacemaker leads, which are routinely used during cardiac surgery today. These are attached to the heart before chest closure, but the small size allows removal through the chest wall several days into the postoperative phase. A sensor encapsulated in biocompatible materials and incorporated in such temporary pacemaker leads, would allow monitoring of the patients also in the interesting period of the first few days following surgery. We will emphasize that this method is not an alternative to trans-thoracic ultrasound imaging, but intended as a tool giving detailed information about the myocardial contraction in special situations when the thorax has been opened for other reasons, i.e. during cardiac surgery.

Conclusion

We have developed an experimental ultrasound system using small transducers directly sutured on the epicardium to measure the heart contraction pattern at high spatial and temporal resolution. We have demonstrated how this can be used to track myocardial deformation and study regional myocardial strain. The velocity-based layer tracking was combined with an automatic boundary detection algorithm to find and track the endocardial border. The high temporal resolution allowed detecting changes in phases during the myocardial motion. The high spatial resolution together with up-sampling and time delay estimation increased the accuracy of the velocity estimates, showing very little drift through the cardiac cycle. The presented study demonstrates the feasibility of the measurement system and the layer tracking method, with emphasis of the technological solution. The main purpose of this study was to develop and investigate the technology, algorithms and the method, and no conclusions about the clinical usefulness are drawn from this study.

Reference

Alshennawy AA, Aly AA. Edge Detection in Digital Images Using Fuzzy Logic Technique. 2009.

Bugge-Asperheim B, Leraand S, Kiil F. Local dimensional changes of the myocardium measured by ultrasonic technique. Scand J Clin Lab Invest 1969;24:361–371.

377 Céspedes I, Huang Y, Ophir J, Spratt S. Methods for estimation of subsample time delays of digitized
378 echo signals. Ultrason Imaging 1995;17:142–171.
379 Choi HF, D'hooge J, Rademakers FE, Claus P. Distribution of active fiber stress at the beginning of
380 ejection depends on left-ventricular shape. Conf Proc Annu Int Conf IEEE Eng Med Biol Soc
381 IEEE Eng Med Biol Soc Annu Conf 2010;2010:2638–2641.
382 Choi HF, Rademakers FE, Claus P. Left-ventricular shape determines intramyocardial mechanical
383 heterogeneity. Am J Physiol Heart Circ Physiol 2011;301:H2351-2361.
384 Chu CH, Delp EJ, Buda AJ. Detecting left ventricular endocardial and epicardial boundaries by digital
385 two-dimensional echocardiography. IEEE Trans Med Imaging 1988;7:81–90.
386 Comunale ME, Body SC, Ley C, Koch C, Roach G, Mathew JP, Herskowitz A, Mangano DT. The
387 concordance of intraoperative left ventricular wall-motion abnormalities and
388 electrocardiographic S-T segment changes: association with outcome after coronary
389 revascularization. Multicenter Study of Perioperative Ischemia (McSPI) Research Group.
390 Anesthesiology 1998;88:945–954.
391 Crescenzi G, Bove T, Pappalardo F, Scandroglio AM, Landoni G, Aletti G, Zangrillo A, Alfieri O.
392 Clinical significance of a new Q wave after cardiac surgery. Eur J Cardio-Thorac Surg Off J
393 Eur Assoc Cardio-Thorac Surg 2004;25:1001–1005.
394 D'hooge J, Heimdal A, Jamal F, Kukulski T, Bijnens B, Rademakers F, Hatle L, Suetens P, Sutherland
395 GR. Regional strain and strain rate measurements by cardiac ultrasound: principles,
396 implementation and limitations. Eur J Echocardiogr J Work Group Echocardiogr Eur Soc
397 Cardiol 2000;1:154–170.
398 D'hooge J, Schlegel J, Claus P, Bijnens B, Thoen J, Werf FV de, Sutherland GR, Suetens P. Evaluation
399 of transmural myocardial deformation and reflectivity characteristics. 2001 IEEE Ultrason
400 Symp Proc Int Symp Cat No01CH37263 2001. pp. 1185–1188 vol.2.
401 Ellis RM, Franklin DL, Rushmer RF. Left ventricular dimensions recorded by sonocardiometry. Circ
402 Res 1956;4:684–688.

Espinoza A, Bergsland J, Lundblad R, Fosse E. Wide sternal retraction may impede internal mammary artery graft flow and reduce myocardial function during off-pump coronary artery bypass grafting: presentation of two cases. Interact Cardiovasc Thorac Surg 2012;15:42–44.

Espinoza A, Halvorsen PS, Skulstad H, Lundblad R, Bugge JF, Hoff L, Fosse E, Edvardsen T. Automated detection of myocardial ischaemia by epicardial miniature ultrasound transducers--a novel tool for patient monitoring during cardiac surgery. Eur J Cardio-Thorac Surg Off J Eur Assoc Cardio-Thorac Surg 2011;39:53–59.

Feng J, Lin WC, Chen CT. Epicardial boundary detection using fuzzy reasoning. IEEE Trans Med Imaging 1991;10:187–199.

Hartley CJ, Latson LA, Michael LH, Seidel CL, Lewis RM, Entman ML. Doppler measurement of myocardial thickening with a single epicardial transducer. Am J Physiol 1983;245:H1066-1072.

Hoff L, Espinoza A, Ihlen H. Cardiac monitoring using transducers attached directly to the heart. 2008 IEEE Ultrason Symp 2008. pp. 749–752.

Hyler S, Pischke SE, Halvorsen PS, Espinoza A, Bergsland J, Tønnessen TI, Fosse E, Skulstad H. Continuous monitoring of regional function by a miniaturized ultrasound transducer allows early quantification of low-grade myocardial ischemia. J Am Soc Echocardiogr Off Publ Am Soc Echocardiogr 2015;28:486–494.

Kass M, Witkin A, Terzopoulos D. Snakes: Active contour models. Int J Comput Vis 1988;1:321–331.

Kowalski M, Kukulski T, Jamal F, D'hooge J, Weidemann F, Rademakers F, Bijnens B, Hatle L, Sutherland GR. Can natural strain and strain rate quantify regional myocardial deformation? A study in healthy subjects. Ultrasound Med Biol 2001;27:1087–1097.

Kukulski T, Jamal F, D'Hooge J, Bijnens B, De Scheerder I, Sutherland GR. Acute changes in systolic and diastolic events during clinical coronary angioplasty: a comparison of regional velocity, strain rate, and strain measurement. J Am Soc Echocardiogr Off Publ Am Soc Echocardiogr 2002;15:1–12.

Kukulski T, Jamal F, Herbots L, D'hooge J, Bijnens B, Hatle L, De Scheerder I, Sutherland GR. Identification of acutely ischemic myocardium using ultrasonic strain measurements. A clinical study in patients undergoing coronary angioplasty. J Am Coll Cardiol 2003;41:810–819.

Landesberg G, Mosseri M, Zahger D, Wolf Y, Perouansky M, Anner H, Drenger B, Hasin Y, Berlatzky Y, Weissman C. Myocardial infarction after vascular surgery: the role of prolonged stress-induced, ST depression-type ischemia. J Am Coll Cardiol 2001;37:1839–1845.

Ludbrook GL, Russell WJ, Webb RK, Klepper ID, Currie M. The Australian Incident Monitoring Study. The electrocardiograph: applications and limitations--an analysis of 2000 incident reports. Anaesth Intensive Care 1993;21:558–564.

Matre K, Fanneløp T, Dahle GO, Heimdal A, Grong K. Radial strain gradient across the normal myocardial wall in open-chest pigs measured with doppler strain rate imaging. J Am Soc Echocardiogr Off Publ Am Soc Echocardiogr 2005;18:1066–1073.

Matre K, Moen CA, Fanneløp T, Dahle GO, Grong K. Multilayer radial systolic strain can identify subendocardial ischemia: an experimental tissue Doppler imaging study of the porcine left ventricular wall. Eur J Echocardiogr J Work Group Echocardiogr Eur Soc Cardiol 2007;8:420–430.

Nguyen TT, Espinoza AW, Remme EW, D'hooge J, Hoff L. Transmural myocardial strain distribution measured at high spatial and temporal resolution. 2011 IEEE Int Ultrason Symp 2011. pp. 696–699.

Setarehdan SK, Soraghan JJ. Automatic cardiac LV boundary detection and tracking using hybrid fuzzy temporal and fuzzy multiscale edge detection. IEEE Trans Biomed Eng 1999;46:1364–1378.

Skulstad H, Urheim S, Edvardsen T, Andersen K, Lyseggen E, Vartdal T, Ihlen H, Smiseth OA. Grading of myocardial dysfunction by tissue Doppler echocardiography: a comparison between velocity, displacement, and strain imaging in acute ischemia. J Am Coll Cardiol 2006;47:1672–1682.

Smith JS, Cahalan MK, Benefiel DJ, Byrd BF, Lurz FW, Shapiro WA, Roizen MF, Bouchard A, Schiller NB. Intraoperative detection of myocardial ischemia in high-risk patients:

electrocardiography versus two-dimensional transesophageal echocardiography. Circulation 1985;72:1015–1021.

Weidemann F, Eyskens B, Jamal F, Mertens L, Kowalski M, D'Hooge J, Bijnens B, Gewillig M, Rademakers F, Hatle L, Sutherland GR. Quantification of regional left and right ventricular radial and longitudinal function in healthy children using ultrasound-based strain rate and strain imaging. J Am Soc Echocardiogr Off Publ Am Soc Echocardiogr 2002;15:20–28.

Yu C-M, Sanderson JE, Marwick TH, Oh JK. Tissue Doppler imaging a new prognosticator for cardiovascular diseases. J Am Coll Cardiol 2007;49:1903–1914.

Directive 2010/63/EU of the European Parliament and of the Council of 22 September 2010 on the protection of animals used for scientific purposes Text with EEA relevance. 276, 32010L0063 Oct 20, 2010. Available from: http://data.europa.eu/eli/dir/2010/63/oj/eng

Figure captions

Figure 1: The open chest porcine experiment. Two sensors were sutured to the epicardial surface of the left ventricle in the apical region and in the basal region. In order to reduce number of animal experiments the experimental protocol also included attachment and testing of accelerometer sensors as part of a different study.

Figure 2: Schematic illustration of the main parts of the measurement system. Two transducers sutured to the heart are connected to the analog ultrasound transmit-receive system. The signals from this are digitized and transferred to a computer. ECG and pressure catheter signals are sampled simultaneously, and synchronized with the ultrasound recordings using pulses from an analog output (DAC).

Figure 3: Flow-chart illustrating the velocity estimation. The RF-lines were filtered and up-sampled 10 times, and cross-correlation was applied to find the time-shift giving the velocity as function of depth.

Figure 4: Diagram of boundary detection method based on intensity of M-mode image. The first estimate for the endocardial border was found from a fuzzy logic technique and boundary search steps. This estimate was refined and smoothened by a maximum filter along the time, removing outliers based on maximum velocity, and applying snake algorithm in the time direction.

Figure 5: Illustration of the fuzzy logic definitions. A pixel is associated a value 0, 'black' or 1, 'white' depending on the grey level of the M-mode image relative to the thresholds a and b.

Figure 6: The range of 20 RF lines after Hilbert transform and log compression mapped to gray scale of range [0 255].

Figure 7: Gray scale M-mode image with the detected endocardial border. Results before (a) and after (b) removing outliers and applying the snake algorithm. (a): The endocardial border first found from the fuzzy logic algorithm and boundary search (blue) and after applying the maximum filter (red) to the blue curve. (b): Result after removing outliers based on maximum velocity and applying the snake algorithm to the red curve in (a), with no requirements (blue), and requiring monotonous expansion during systole (red).

Figure 8: Estimated radial velocity inside the myocardium near the apex (top panel) and the base (bottom panel). No velocity filter was applied. The end-systole is marked with blue vertical lines, and the end-diastole with magenta lines. Synchronously measured ECG (blue) and LV pressure (red) are shown below. The ECG recording was of rather low quality, but sufficient for timing.

Figure 9: M-mode gray scale images with the motion of the detected endocardial border (thick curves) and the four layers (thin curves) inside the myocardium as overlays near the apex (top) and the base (bottom). The curves are calculated from the velocity patterns in Figure 8 by tracking the motion in the forward direction.

Figure 10: M-mode gray scale images with the motion of the detected endocardial border (thick curves) and the four layers (thin curves) inside the myocardium as overlays near the apex (top) and near the base (bottom). The curves were calculated from the unfiltered velocity patterns in Figure 8 by combining data from tracking the motion in the forward and backward directions, assuming periodic motion.

Figure 11: Estimated radial strain of four layers inside the myocardium near the apex (top) and the base (bottom). Layers are numbered in increasing order from the subepicardial layer 1 to the subendocardial layer 4. The strain curves were computed from the velocity patterns in Figure 8 combining with myocardial layers in Figure 10.

Tables

Table 1: Parameters for endocardial boundary detection for myocardium. Two transducers were used, 'Transducer 1' was positioned near the apex and 'Transducer 2' was positioned near the base of the heart.

		Transducer 1 Apex	Transducer 2 Base
Thresholds [*a*, *b*] for fuzzy logic processing		[158.1 196.35]	[140.25 214.2]
Depth range for searching the endocardial boundary		10 mm to 18 mm	10 mm to 19.98 mm
Snake algorithm parameters	α	5000	5000
	β	0	0
	γ	10	10
	Iterations	1000	500
Assume monotonous expansion during systole		No	Yes

Figure1

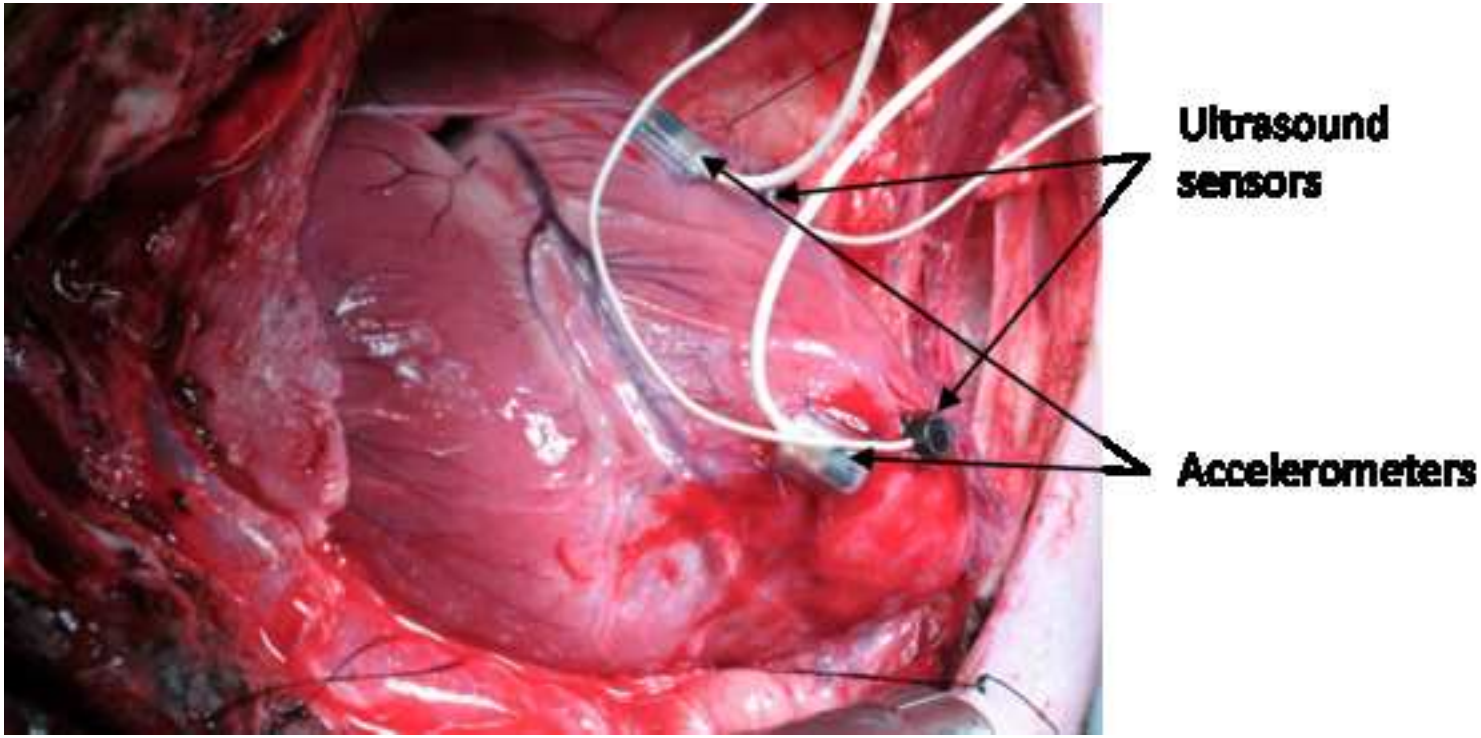

Figure2

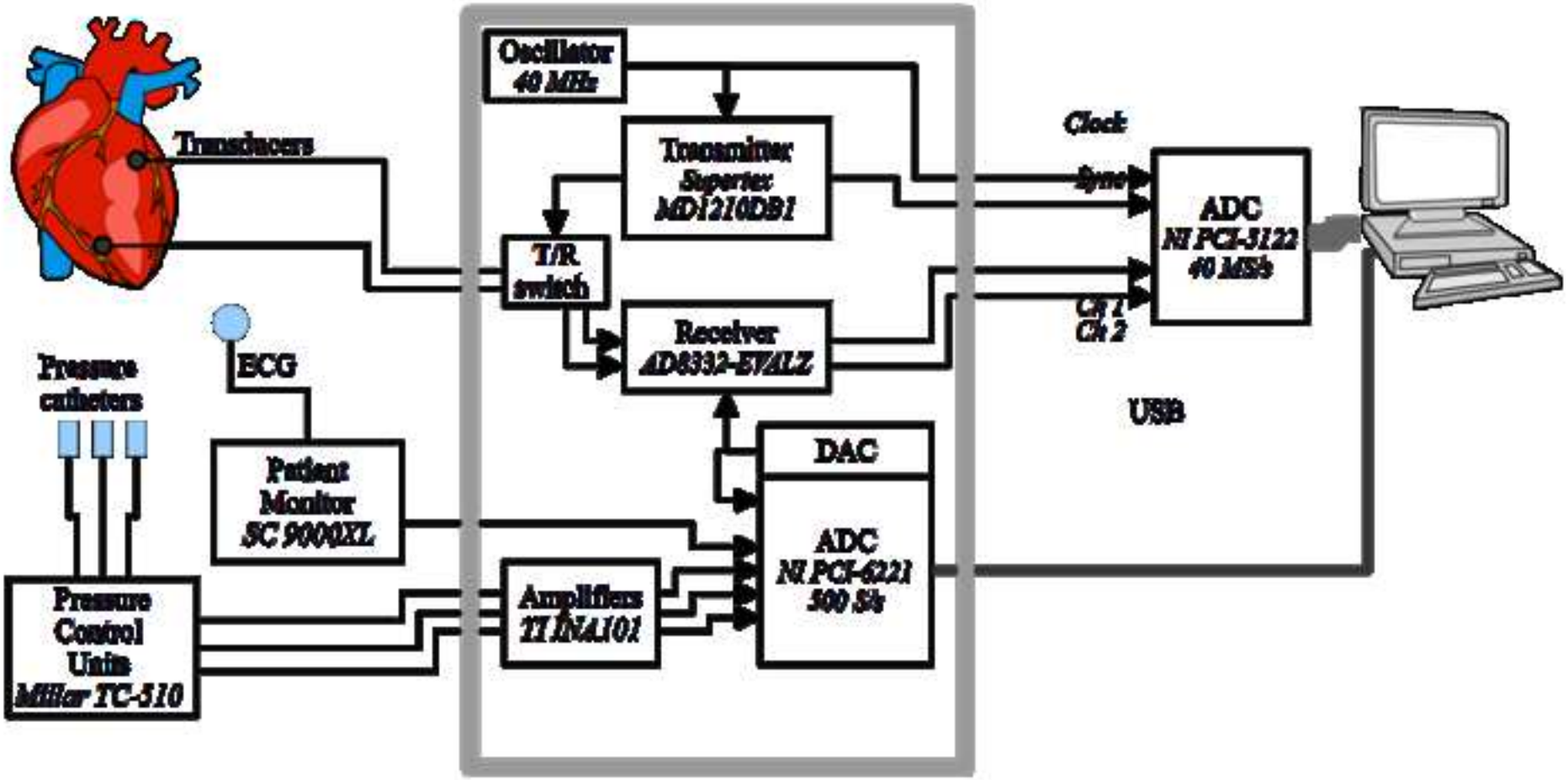

Figure3

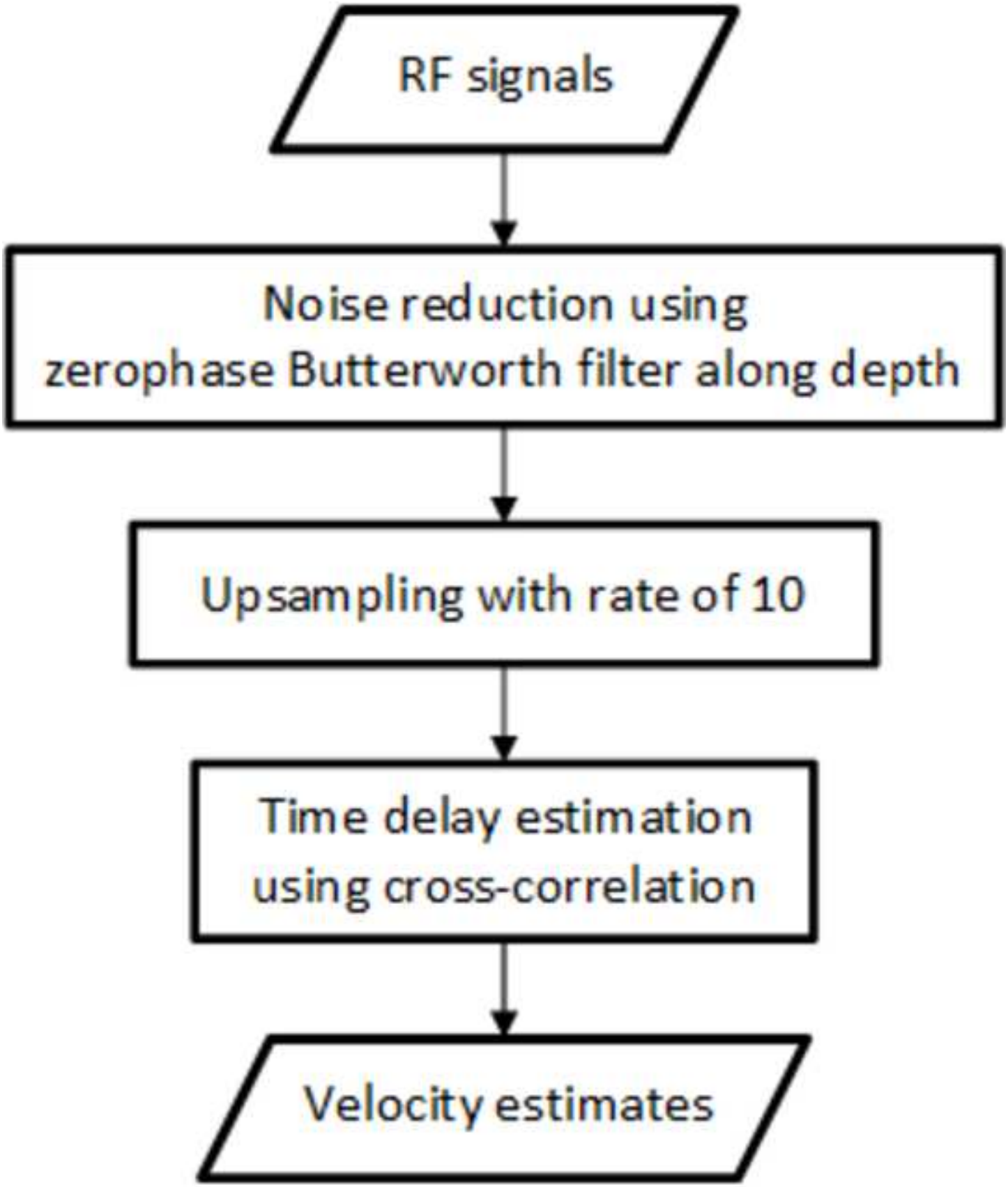

Figure4

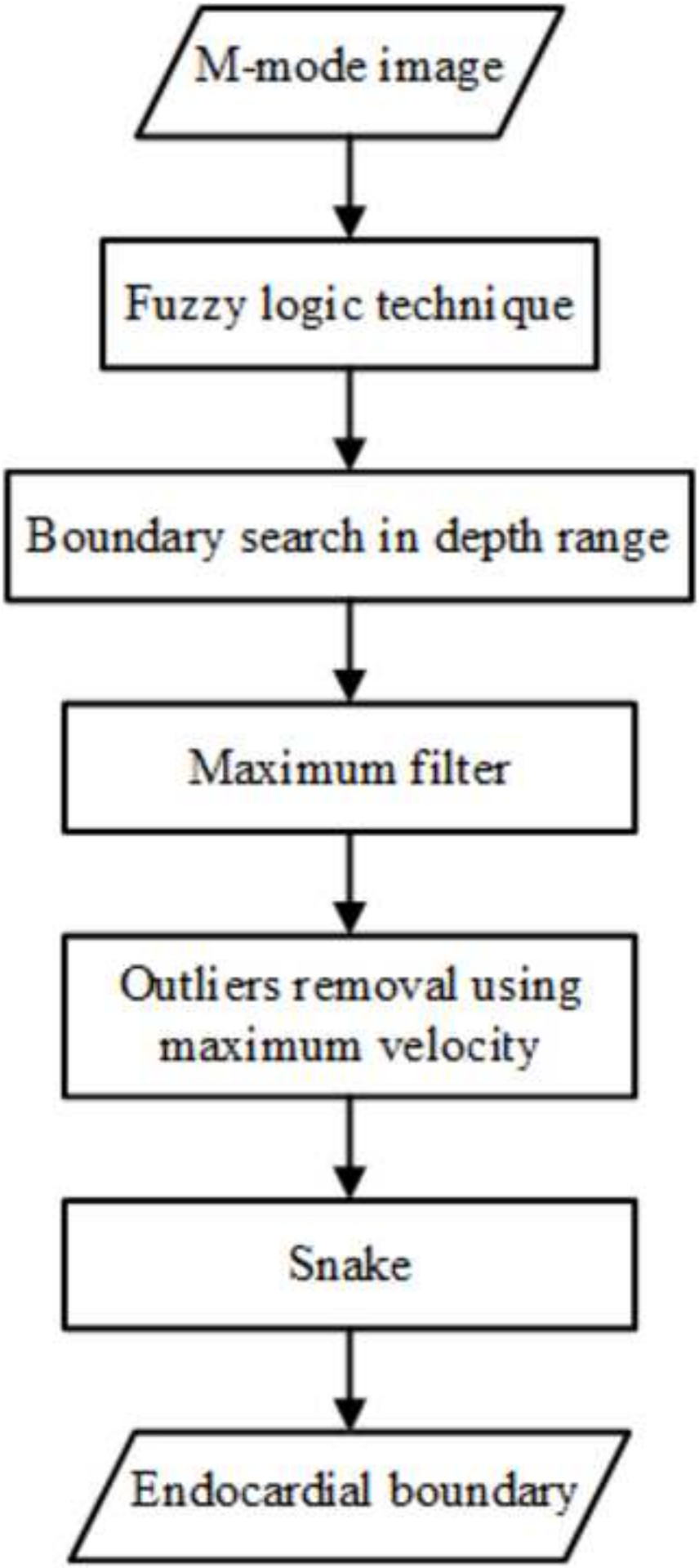

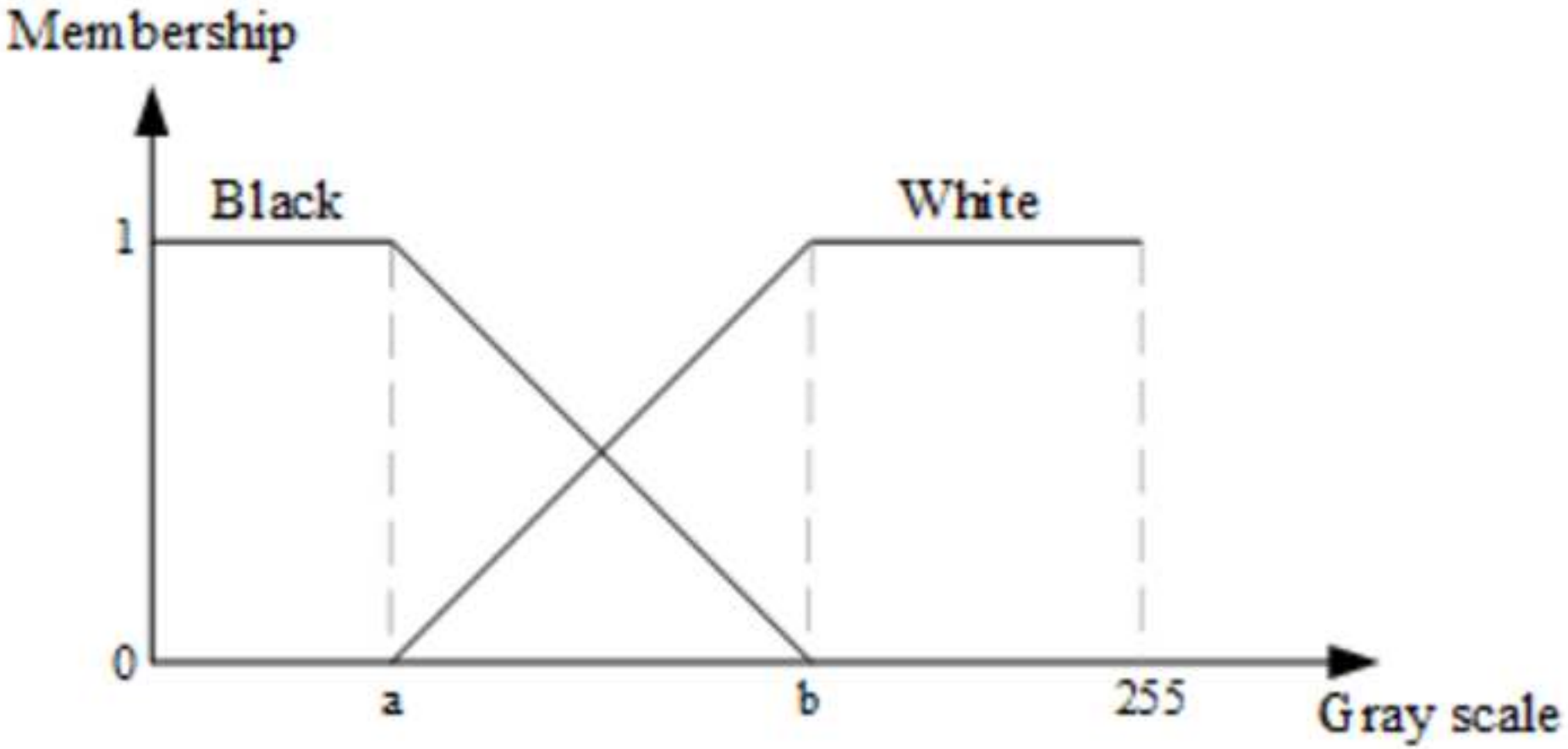

Figure6

Click here to access/download;Figure;Figure6.tif

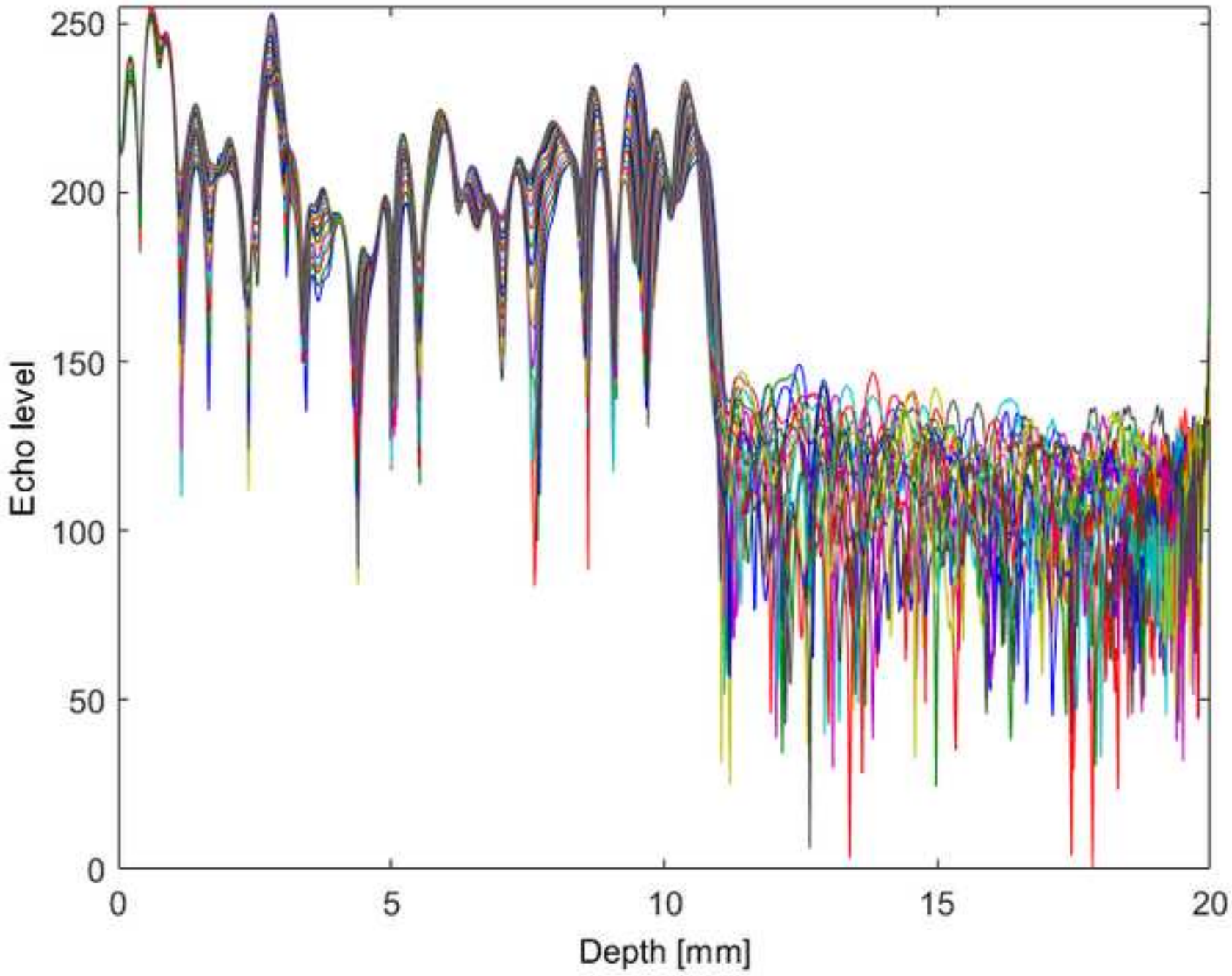

Figure7

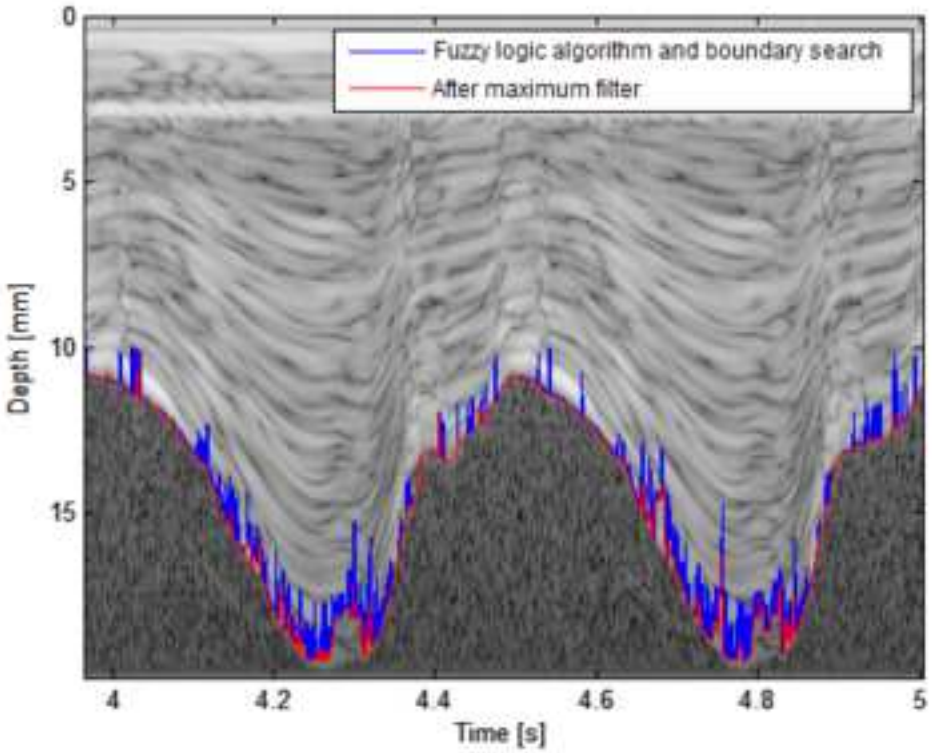

(a)

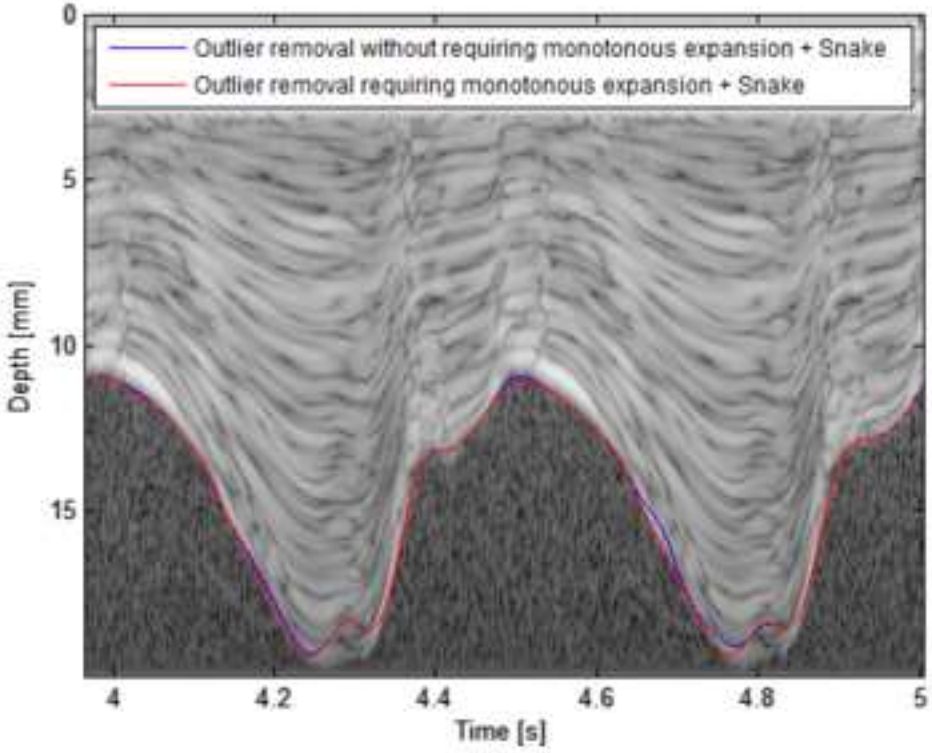

(b)

Figure8

Click here to access/download;Figure;Figure8.tif

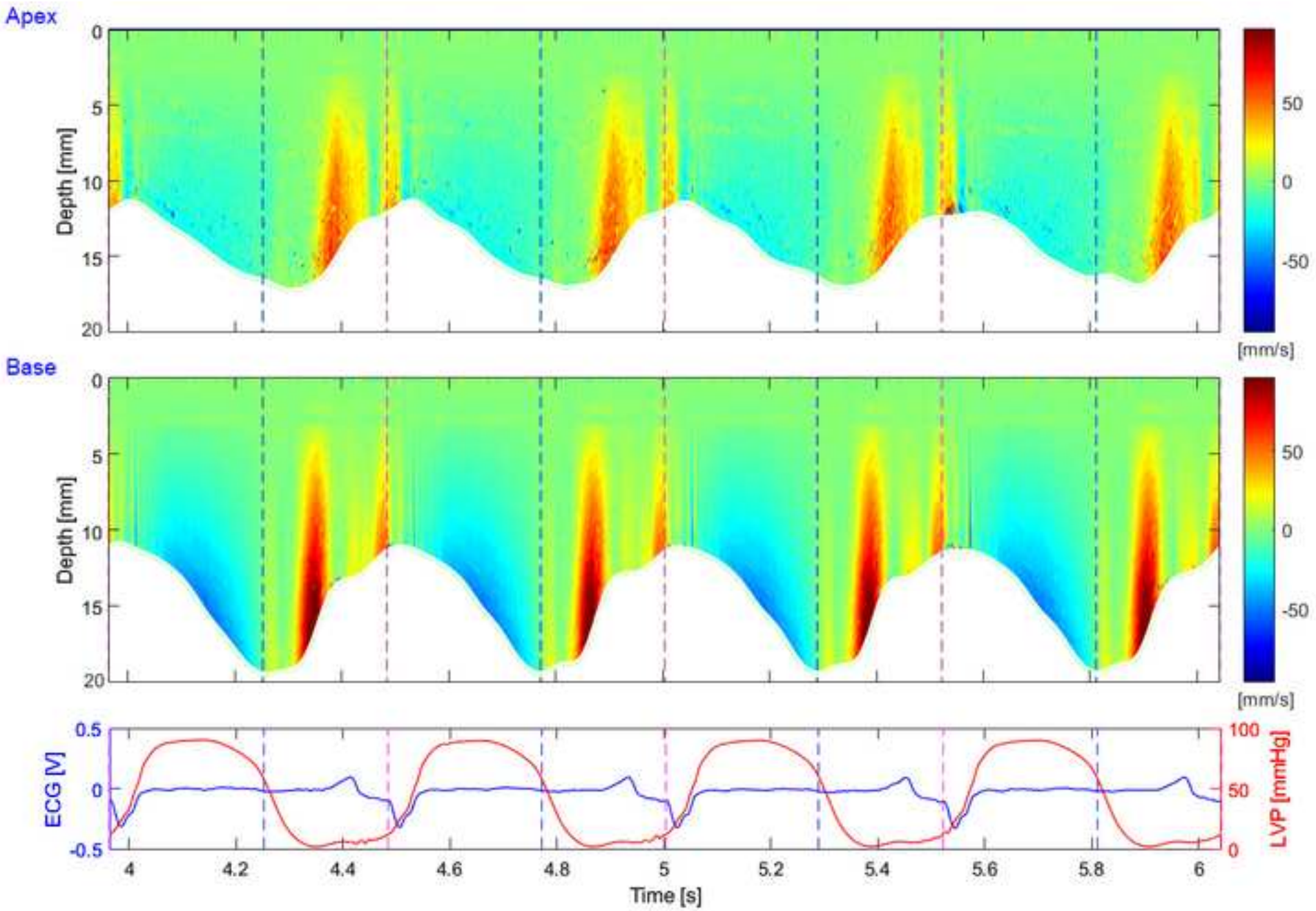

Figure9

Click here to access/download;Figure;Figure9.tif

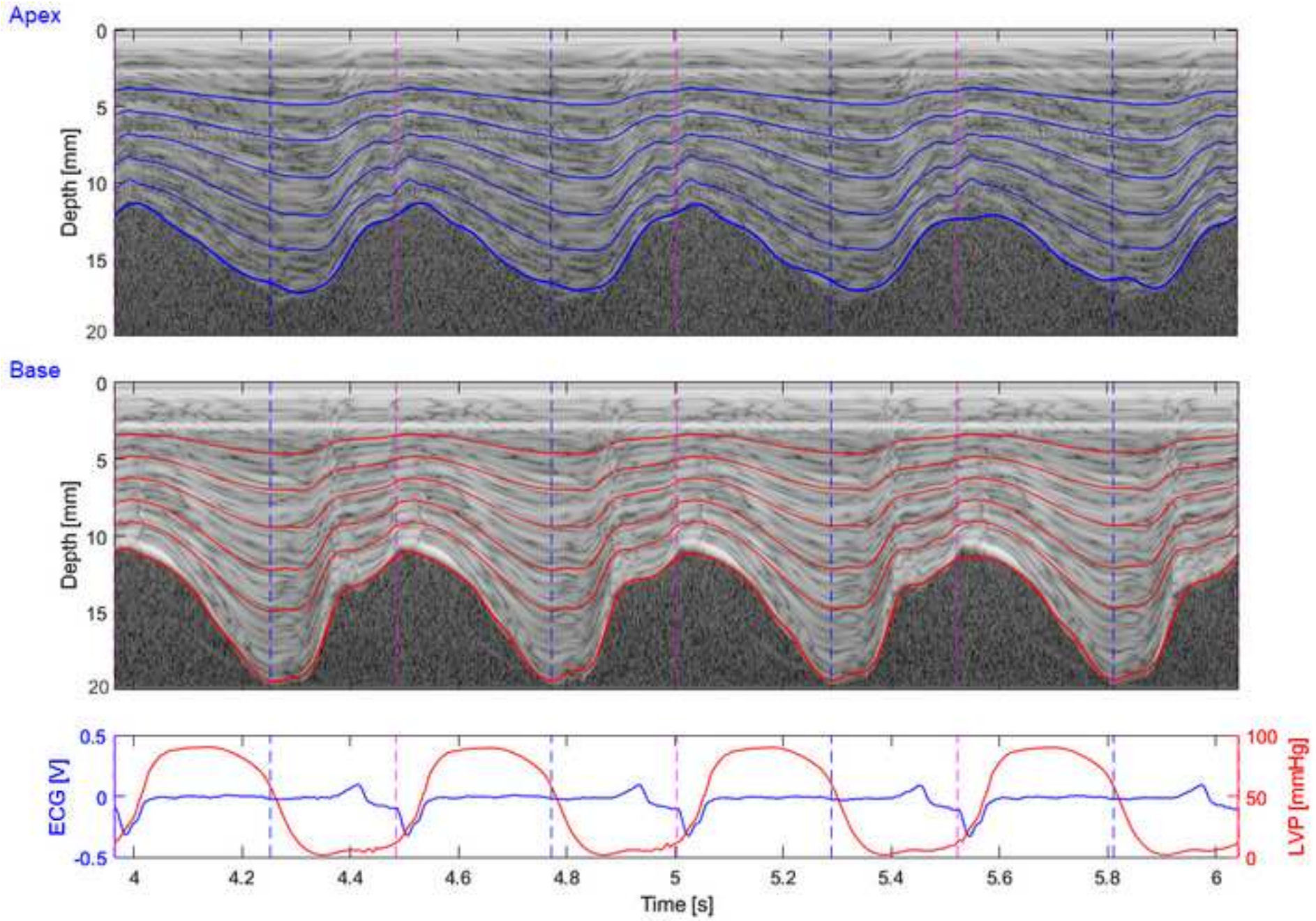

Figure10

Click here to access/download;Figure;Figure10.tif